PAPER • OPEN ACCESS

Exploration of the charge transport mechanism, complex impedance, dielectric/electric modulus and energy storage characteristics of the aloe vera (*Aloe Barbadensis Miller*) plant

To cite this article: Maria Vesna Nikolic *et al* 2024 *Mater. Res. Express* **11** 016302

Materials Research Express

PAPER

Exploration of the charge transport mechanism, complex impedance, dielectric/electric modulus and energy storage characteristics of the aloe vera (*Aloe Barbadensis Miller*) plant

Maria Vesna Nikolic[1,*], **Charanjeet Singh**[2,*] **and Milica Bogdanovic**[3]

[1] University of Belgrade—Institute for Multidisciplinary Research, Kneza Viseslava 1, 11030 Belgrade, Serbia
[2] School of Electronics and Electrical Engineering, Lovely Professional University, Phagwara Punjab, India
[3] Institute for Biological Research 'Sinisa Stankovic'—National Institute of Republic of Serbia, University of Belgrade, Bulevar Despota Stefana 142, 11060 Belgrade, Serbia
[*] Authors to whom any correspondence should be addressed.

E-mail: mariavesna@imsi.bg.ac.rs, rcharanjeet@gmail.com and milica.bogdanovic@ibiss.bg.ac.rs

Keywords: aloe vera, impedance, dielectric properties, electrical properties

OPEN ACCESS

RECEIVED
3 August 2023

REVISED
7 December 2023

ACCEPTED FOR PUBLICATION
4 January 2024

PUBLISHED
15 January 2024

Abstract

Complex impedance spectra at room temperature in the frequency range of 8 Hz—5 MHz were measured on freshly cut leaf sections of the Aloe vera plant by AC impedance spectroscopy. They were analyzed using a classical 'brickwork' equivalent circuit composed of grain and grain boundary contributions commonly applied to solid-state materials. The obtained grain resistance/capacitance was 0.4 MΩ/72 pF and grain boundary resistance/ capacitance was 66.4 MΩ/50 nF. The determined conductivity changed according to the Jonscher power law with σ_{DC} of $4.02 \cdot 10^{-5}$ $(\Omega m)^{-1}$ and frequency constant of 0.92 characteristic for hopping as the conduction mechanism. Analysis of dielectric permittivity and electric modulus confirmed the non-Debye relaxation behavior. Nyquist plots for electric modulus revealed conductivity relaxation in the low frequency attributed to grain boundaries and impedance modulus displayed dielectric relaxation in the high frequency region associated with grains. A correlation has been established among the investigated parameters, morphology, and EIS-derived simulated parameters.

1. Introduction

Aloe vera (*Aloe barbadensis Miller*) is a succulent perennial plant species, from the *Asphodelaceae* family and *Aloe* genus [1]. It grows and thrives in hot and dry climates. Its leaves are thick and fleshy enabling the plant to store water [2]. Plant survival is dependent on the pulp beneath the leaf which stores water as well as nutrients. The thick wax-like outer layer of the leaf impedes water from evaporation. Succulence is a feature of crassulacean acid metabolism plants with a specific pathway of carbon fixation enabling survival and even growth under conditions with not a lot of water [3]. Aloe leaves are dark green in color, well-connected at the stem in a whirling rosette structure [4]. The thick epidermis causes the leaf formation- an outer green protective rind covered by cuticle encompassing the mesophyll. The inner latex layer contains vascular bundles. The mesophyll is differentiated into chlorenchyma and thinner-walled parenchyma (pulp-fillet) cells [4]. The parenchyma cells constitute a transparent mucilaginous jelly generally mentioned as Aloe vera gel. The water content in raw pulp is ~98.5%, while it is ~99.5% in the gel [5]. Polysaccharides make up more than 60% of the remaining solid part [6], while the remaining compounds are glycoproteins, enzymes, water-soluble and fat-soluble vitamins, minerals, phenolic compounds, such as anthraquinones, and organic acids [7]. Aloe vera leaves contain minerals, such as Ca, Mg, Na, K, P, Fe, Cu, Zn, and Mn [4, 8]. Aloe vera is used traditionally in medicine, as it has shown wound and burn healing properties, anti-inflammatory, and immunomodulatory effects [5]. Aloe vera gel is widely applied in the medicine and pharmaceutical industry [7, 8], food industry as food coating [9] and textile industry [10]. Aloe vera fibers have been investigated as lignocellulosic fibers for reinforcing biopolymers such as polylactic acid (PLA) for application in green composites [11].

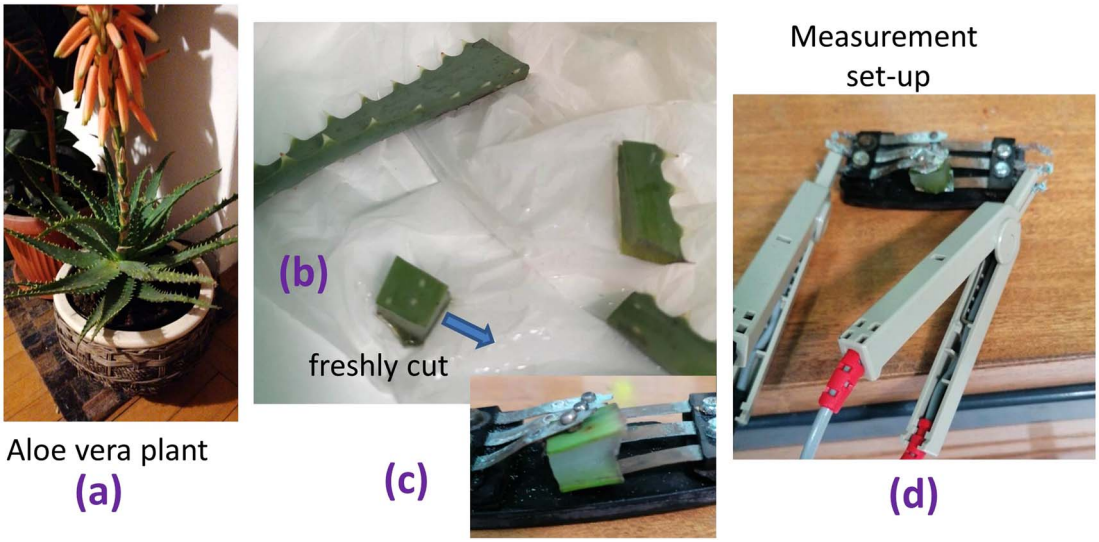

Figure 1. Aloe vera plant (a), freshly cut leaf samples (b), and leaf sample placed in the sample holder for impedance measurement (c) and (d).

Recent research has focused on plants in two ways: the first is design of plant based biohybrid systems and the second is the growing field of bioelectronics tailored for plant health monitoring [12]. Biohybrid systems use plants as integral parts of a device or functionalize plants with smart materials and transform them into biohybrid devices. Biohybrids have a wide range of applications including energy harvesting, self-organized electronics and plant nanobionics [12–15]. Thus, recent research by Alluri *et al* [16] has focused on using Aloe vera gel as an active component of a piezo-electric energy harvester, while Mousa *et al* [17] used Aloe vera pulp to design a soft e-skin biohybrid for tactile sensing. Bioimpedance spectroscopy has been used to measure and interpret plant electrical signals and monitor plant behavior [12, 18]. When monitoring plant health the applied electrode can disturb the natural processes occurring in the plant and on the plant surface. Thus Kim *et al* [19] applied a vapor-tissue polymer tattoo electrode to monitor deep tissue damage in living hosta plants, while Barbosa *et al* [20] attached wearable sensors to leaves to monitor plant water loss.

Electrical impedance spectroscopy (complex resistance $(R + jX)$ measured during application of an alternating current (AC) is a method widely applied to characterize solid-state materials, including ceramics, solid state electrolytes and polymers [21–24]. This method has been applied to other solid materials, including biological tissues. Electrical conductivity in biological tissues has been linked with ion content and ionic mobility [25]. In plants, measurements using electrical impedance spectroscopy have been done to monitor plant health status [25, 26]. The impedance of plant tissue was found to be dependent on membrane structures, cellular ionic content, and viscosity [25]. Focusing on Aloe vera, inspired by the versatility and applicability of this succulent plant, its water retention ability and the significance of both bioelectronic and biohybrid research, we performed a study of complex impedance change with frequency (range 8 Hz—5 MHz) on freshly cut leaf sections of a healthy well-watered Aloe vera plant, without applying any additional electrode. By applying a classical 'brickwork' equivalent circuit model [21, 27] we observed it as a solid-state material with grains and grain boundary resistance/capacitance contributing to the change in impedance with frequency and identified the low frequency electrode effect. This research is the first step in establishing a correlation between the biological and electrical properties through circuit modeling and sample microstructure and ascertaining the origin of the water retention ability in succulents, such as Aloe vera in order to better understand the energy harvesting ability of succulents as possible renewable sources of energy.

2. Materials and methods

The Aloe vera (*Aloe barbadensis Miller*) plant was purchased in a local greenhouse flower shop, as shown in figure 1. Freshly cut leaf pieces were used for measurement as shown in figure 1. The sample dimensions were 11×11 mm (surface) and 8 mm (thickness). Samples were placed into a sample holder (made in our laboratory with copper components and generally used for measuring electric and dielectric properties of pellet samples in parallel plate capacitor mode) as shown in figure 1. The actual contact copper electrode had a diameter of 3 mm. The sample impedance $(R + jX)$ and phase angle were measured in the same way as for ceramic pellet samples. We used a HIOKI LCR 3536 analyzer (Nagano, Japan) with a basic accuracy Z ± 0.05% rdg. θ: ±0.03°

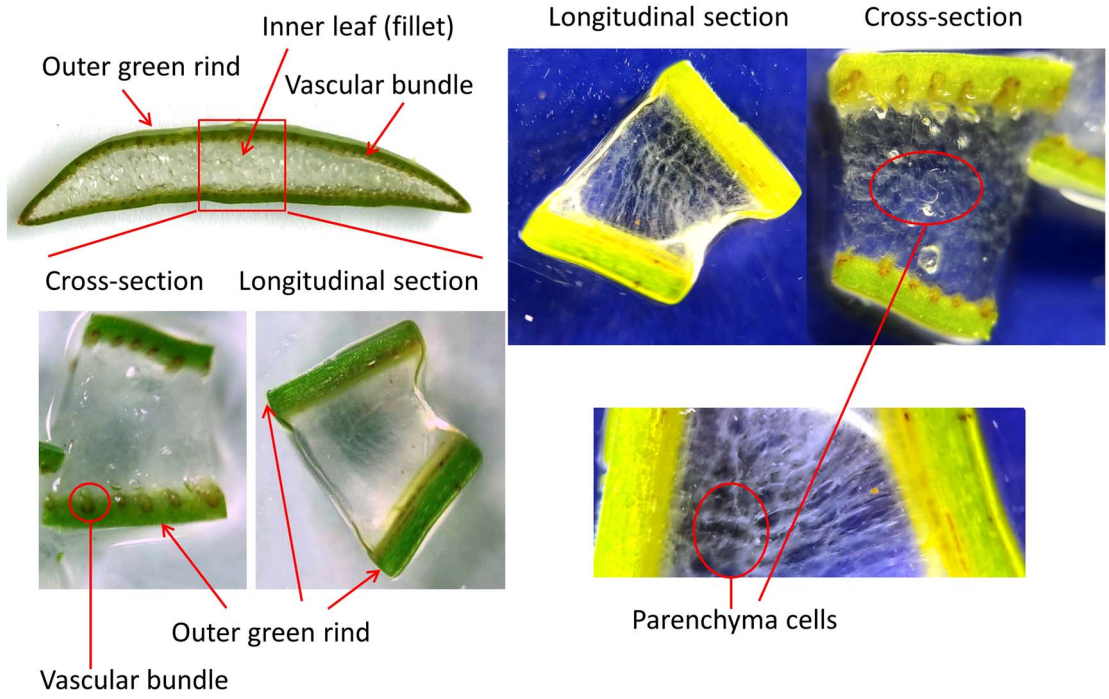

Figure 2. Optical microscopy images of the cross and longitudinal leaf sections of freshly cut Aloe vera leaf.

(representative value, measurable range: 1 mΩ to 200 MΩ), frequency range 8 Hz—5 MHz − 5 digits setting resolution, minimum resolution 10 mHz). The measurements were conducted at room temperature (25 °C) in the frequency range 8 Hz—5 MHz. The applied voltage was 1 V and this value was selected as a common value applied when measuring ceramic pellet samples or thick films [28]. The current through the sample during such AC voltage is commonly in the range 2 mA—0.2 μA depending on the frequency value and measured impedance. The instrument and sample holder were connected with a 4-TERMINAL PROBE 9140–10 accessory. We measured 200 points distributed in a logarithm distribution in the measured frequency range with 1 s between each measurement. All measurements were done in triplicate.

Leaf sections for illustration of the leaf structure were prepared by free-hand sectioning. Samples of the middle region of the leaf, about 4 mm wide and 10 mm long, were cut. Cross and longitudinal sections (about 4 × 3 mm, thickness about 1 mm) of these samples were prepared by free-hand sectioning with a razor blade. The prepared sections were moved into a drop of distilled water placed on a microscope slide. Tissue paper was used to partially absorb excess water. Samples were photographed using a Redmi Note 9Pro cell phone with a 64MP Quad camera with a clip-on macro lens 12.5× lighted by a dual LED light source.

Samples for FTIR analysis were prepared by freeze-drying freshly cut leaf samples for 48 h. This method enabled the removal of all liquid (water) from the sample, leaving only dry tissue and rind. FTIR spectra of the outer rind and fluffy inner leaf cell structure were recorded on a Perkin Elmer Spectrum Two (Waltham MA, USA) in the range 400–4000 cm^{-1}, resolution 8 cm^{-1}. All measurements were performed in triplicate.

3. Results and discussion

3.1. Optical microscopy images

In optical microscopy images of Aloe vera leaf cross and longitudinal sections (figure 2), we can see the outer green rind, vascular bundles, and the fillet inner leaf structure. The inner leaf structure is composed of the cell wall, organelle, and gel (transparent mucilaginous jelly) [29]. The images of leaf cross and longitudinal sections show the structure of parenchyma cells showing cell walls with the gel inside. A higher magnitude image of the fillet microstructure has been previously obtained using scanning electron microscopy and has shown that the parenchyma cell size is 300–400 μm [6]. Choi *et al* [29] compared optical and scanning electron microscopy with cryo-scanning electron microscopy of Aloe vera leaf sections. Cryo-scanning electron microscopy enabled observation of the 'near life-like' state of the leaf gel as moisture was retained if the preparation process included rapid sublimation. Beehive-like pores were noted, and the cell structure was preserved showing cells surrounded by cell walls, visible contact surfaces among neighboring cells, and the intercellular space, confirming the cell size to be about 300–400 μm [29].

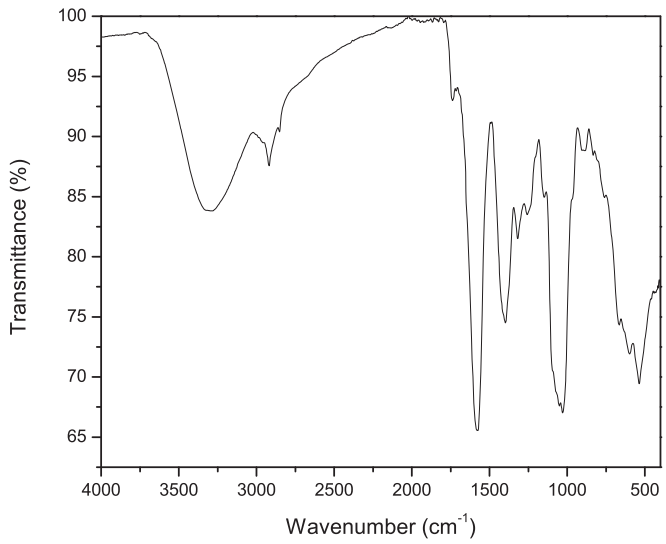

Figure 3. FTIR spectrum of a freeze-dried Aloe vera leaf sample.

3.2. FTIR spectrum analysis

FTIR spectroscopy has been applied to identify the functional groups present in the Aloe vera leaf [2]. We measured FTIR spectra in different parts of the freeze-dried leaf sample and they were very similar showing the same bands with slightly different intensities as noted before in literature for the spectrum of dry Aloe vera gel measured by Dehgan *et al* [30] or aqueous extracts of different Aloe vera samples collected in different regions in India [2]. An example taken of a freeze-dried inner part is given in figure 3. Analysis of the recorded spectra show that the region 3500–3200 cm^{-1} with a wide band centered at ≈3300 cm^{-1} relates to O–H stretching of phenols and carboxylic acids [2]. According to Torres-Giner *et al* [31], the presence of this band in dried Aloe vera samples can be associated with phenolic groups of anthraquinones, such as aloin and emodin. The smaller, but sharper band centered at ≈2919 cm^{-1} with a small shoulder peak at ≈2853 cm^{-1} can be associated with asymmetric as well as symmetric C–H stretching of methylene [31, 32]. The notable band centered at ≈1586 cm^{-1} lies in the C–C in-ring stretching region of aromatics [2], but is also related to asymmetric −COO stretching that combined with a symmetric stretching band at ≈1401 cm^{-1} can be attributed to carboxylate compounds [30]. A low-intensity C=O carbonyl stretching band can also be noted at ≈1738 cm^{-1}. It is accompanied by a low-intensity C–O–C stretching vibration band at 1254 cm^{-1} that can be attributed to *O*-acetyl ester [31]. The intense band at ≈1021 cm^{-1} has been attributed to C–O and C–OH bonds in glucan units in polysaccharides, while the shoulder at ≈1041 cm^{-1} can be attributed to pectin side chains [31, 32]. The bands in the region 700–515 cm^{-1} have been associated with alkynes and alkyl halides [2].

3.3. Complex impedance analysis

The measured impedance ($|Z| = R + jX$, $Z' = R$ is resistance, $Z'' = X$ is reactance) and phase angle of Aloe vera samples are shown in figure 4. According to the shape of the impedance curve, the Aloe vera sample behaves like a solid-state material: ceramic, powder, or electrolyte decreasing as the frequency increases [21–23].

The Nyquist plot of measured complex impedance of Aloe vera leaf sample in the frequency range 8 Hz—5 MHz is shown in figure 5 and resembles the shape of complex impedance spectra of solid state materials [21]. Joczak *et al* [25] concluded that plant tissue impedance in the frequency range 10 Hz—1 MHz is influenced by cell membrane capacitance, intracellular (symplastic) resistance, and intercellular (apoplastic or extracellular) resistance. They proposed different electrical circuits to model the measured impedance, to take into account these influences. Complex impedance spectra of solid-state materials are commonly analyzed using the 'brickwork' model of grain, grain boundary, and electrode-interface regions in the measured frequency range [21, 27]. Each region is modeled with a parallel resistance/capacitor element, representing one semicircle in the complex impedance measurement data semicircles [21]. However, in polycrystalline samples, these semicircles often overlap and are not ideal [33, 34]. If the semicircle center is below the *x*-axis, this is due to non-ideal type Debye behavior, and a constant phase element (CPE) is used to replace the capacitance component in the parallel circuit [24, 31]. The impedance function of a CPE is [33]:

$$Z_{CPE} = A_{CPE}^{-1}(j\omega)^{-n} \quad (1)$$

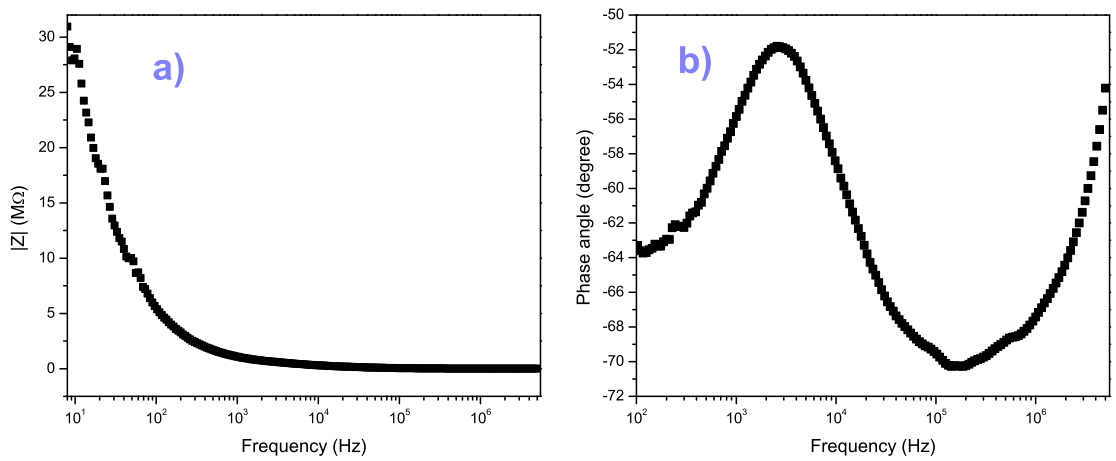

Figure 4. Change of impedance |Z| (a) and phase (b) with frequency measured on an Aloe vera leaf sample.

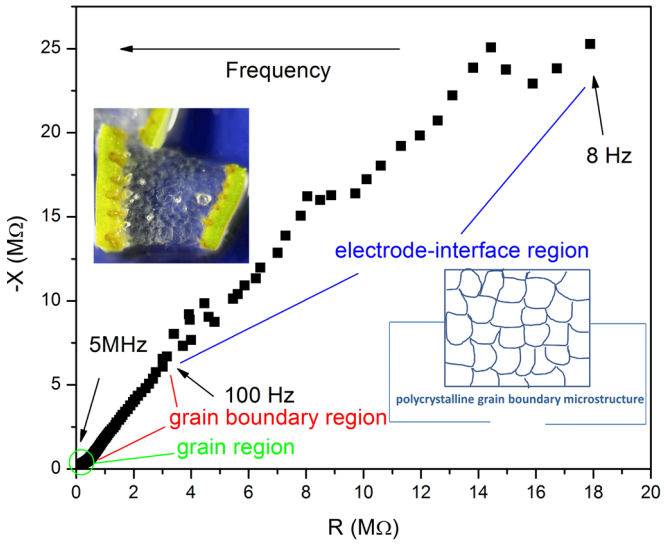

Figure 5. Measured complex impedance of Aloe vera leaf sample, insets: optical microscopy image recorded of a leaf cross-section and illustration of a polycrystalline grain boundary microstructure.

where $\omega = 2\pi f$-angular frequency, f-applied frequency, A_{CPE}-constant independent of frequency (f) and n-an exponential index representing the semicircle arc depression.

The measured complex impedance of Aloe vera has three different regions (figure 5). A small semicircular arc at high frequencies can be noted, followed by a larger part of a semicircular arc in the lower frequency region. If we assume that the Aloe vera microstructure resembles a ceramic sample microstructure with grains and grain boundaries, the small semicircle in the high-frequency region can be modeled with a parallel R/CPE representing the grain contribution, while part of the semicircle arc in the lower frequency region can be modeled with a parallel R/CPE representing the grain boundary contribution, as shown in figures 5 and 6. The complex impedance in the lowest frequency region also reflects the influence of the electrode-interface component that in our case is due to the Aloe vera rind contact with the sample holder copper electrode.

Analysis and simulation of the measured complex impedance spectra were performed using the EIS Spectrum Analyzer software [35] and an equivalent electrical circuit reproducing the influences of grains and grain boundaries on the complex impedance in the frequency range of 100 Hz—5 MHz. The complex impedance data in the measured range 8–100 Hz was the part that reflected the influence of the electrode interface and we did not model it as it was too small to be able to fit with a model, though its shape of a low frequency 'electrode spike' roughly under a 45 ° angle could indicate infinite Warburg-type ionic diffusion [21]. Good agreement between experimental and fitted data was obtained as shown in figure 6. The values of the electric circuit parameters were derived with a fitting error below 2%. The obtained resistance of grain/grain boundary and CPE element values are given in table 1. The real values of grain/grain boundary capacitance were

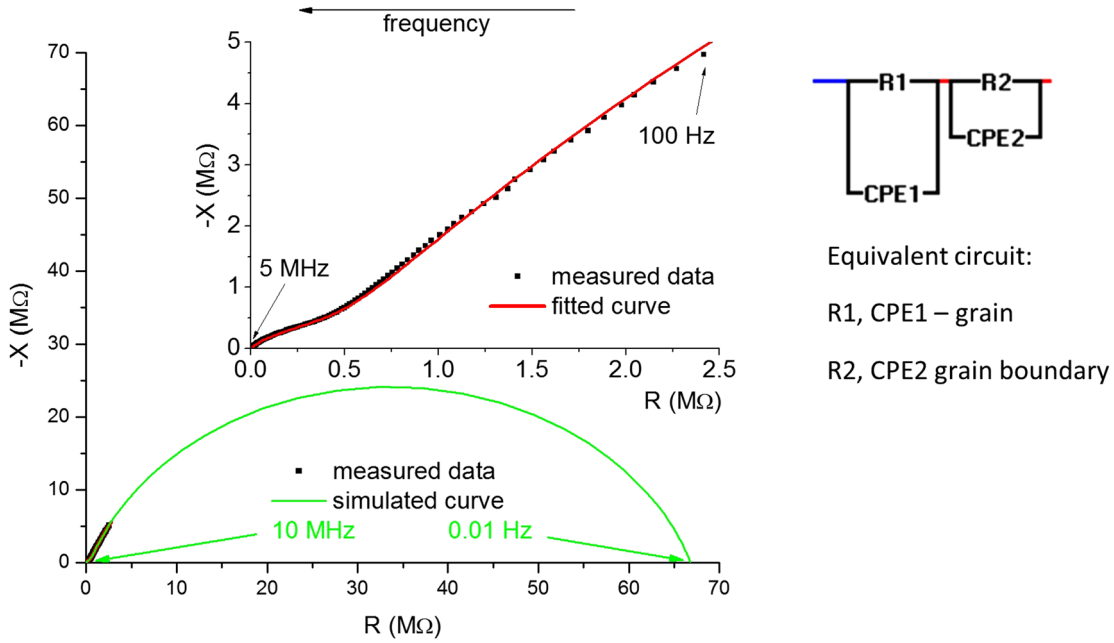

Figure 6. Measured complex impedance data in Nyquist plots, fitted and simulated curves obtained for Aloe vera leaf sample using the applied equivalent circuit consisting of grain and grain boundary components.

Table 1. Grain and grain boundary resistance, CPE equivalent circuit parameters, capacitance, frequency, and time for Aloe vera sample.

	R (MΩ)	A_{CPE}	n	C (F)	f (Hz)	τ (sec)
Grain	0.403	$5.6193 \cdot 10^{-10}$	0.8035	$72.18 \cdot 10^{-12}$	34325.35	$2.913 \cdot 10^{-5}$
Grain boundary	66.42	$9.952 \cdot 10^{-10}$	0.8009	$50.65 \cdot 10^{-9}$	29.71	0.03365

calculated as [22]:

$$C_{CPE} = (A_{CPE} \cdot R^{-(n-1)})^{1/n} \tag{2}$$

where R, $A_{CPE,}$ and n are grain or grain boundary resistance and CPE parameter values determined from the applied model, respectively. It is interesting to observe that the determined capacitance value for grains (C_g) is 72.18 pF and lower than for grain boundaries ($C_{gb} = 50.65$ nF) and in line with grain and grain boundary capacitance values (pF and nF) obtained for solid-state materials, such as ceramics, nanoparticles or solid-state electrolytes [21, 22, 36, 37]. The determined grain boundary resistance (R_{gb}) is also much higher than the determined grain resistance (R_{gb}), so the grain boundaries show higher capacitive and resistive properties than grains in agreement with the microstructure of the Aloe vera fillet, as shown in figure 2 where the cell walls represent grain boundaries and the gel represents grains. Thus, the greater number of grain boundaries observed in microstructure could contribute to larger resistance, while charge carriers accumulate at the grain boundaries causing larger polarization.

3.4. Dielectric properties and conductivity

The complex permittivity was calculated as [22]:

$$\varepsilon' = \frac{X}{|Z|^2\,\omega C_0},\ \varepsilon'' = \frac{R}{|Z|^2\,\omega C_0}, \tag{3}$$

where R and X are the measured real and imaginary components of impedance, $|Z| = \sqrt{R^2 + X^2}$, C_0 is the capacitance of the corresponding air gap parallel plate capacitor with dimensions the same as the measured sample determined as $C_0 = (a^2/d)\cdot\pi\cdot\varepsilon_0$, with a^2—the sample surface, d—sample thickness and ε_0 - permittivity of free space of vacuum. The loss tangent tg δ was determined as: $\varepsilon''/\varepsilon'$. The dependence of dielectric parameters with frequency is similar to conventional synthesized metal-based compounds/oxides/dielectrics as shown in figure 7. Dispersion accompanied by rapid fall in ε' and ε'' in the low-frequency region can be observed showing that electrons can follow the applied signals up to a certain frequency forming the polarization [38]. As the frequency increases the electrons are unable to get in sync and lag behind the applied field [39]. Hence the

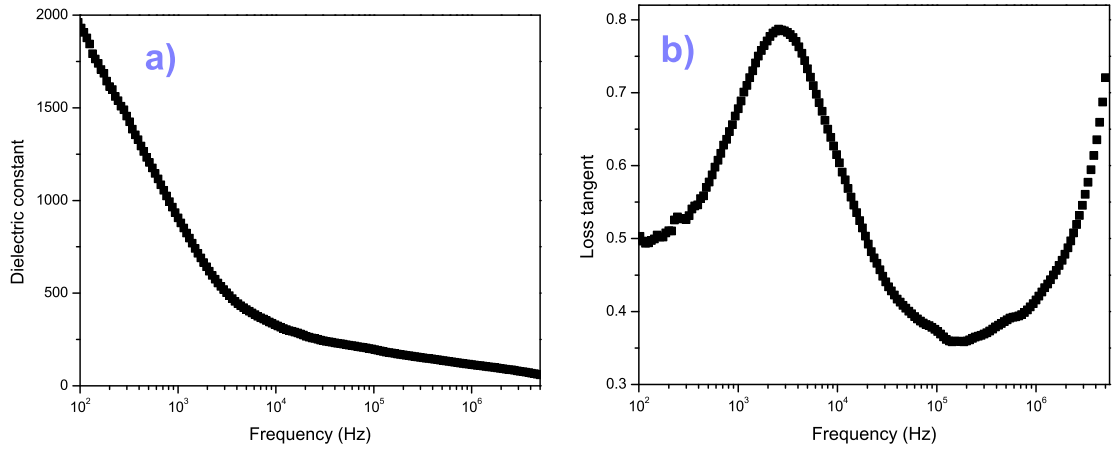

Figure 7. Frequency dependence of the dielectric constant (ε') - (a) and loss tangent (tgD) - (b) determined using equation (3) for measured Aloe vera leaf sample.

polarization suffers reduction, and so do the permittivity components ε' and ε''. For ceramics and powder samples, this trend has been explained by interfacial polarization attributed to an inhomogeneous microstructure and also charge carrier accumulation at boundaries between regions with conductive grains and resistive grain boundaries [22]. The dielectric loss tangent has a maximum similar to the ones noted before for solid-state materials when the frequency of hopping charge carriers corresponds to the external frequency field [22].

The trend of the dielectric constant is also consistent with morphology and EIS-derived parameters. According to Maxwell–Wagner, grain boundaries are prominent at low frequencies and offer resistance to an applied field. The grains are prevalent at high frequencies and assist conductivity. The larger values of C_{gb} and R_{gb} (table 1) cause maximum dielectric constant, Z′ and Z″ values at low frequencies (figures 4 and 7). In the high-frequency regime, low C_g and R_g reduce ε'/Z'' and Z′ respectively (figure 4). Consequently, there is consistency among measured intrinsic parameters, morphology, and EIS-derived simulated parameters.

In the case of conductivity, the Aloe vera sample conductivity was determined as:

$$\sigma = \frac{\varepsilon_0 \cdot R}{C_0 \cdot |Z|^2} \tag{4}$$

where: C_0 is the capacitance of the corresponding air gap parallel plate capacitor with dimensions the same as the measured sample, and ε_0 is the permittivity of free space of vacuum, as described in equation (3), while R is the measured resistance component of the impedance, and $|Z|$ is the mpedance calculated as described in equation (3). The calculated conductivity changed with frequency, as shown in figure 8.

According to the Jonscher power law it can be expressed with the following relation [40]:

$$\sigma(f) = \sigma_{DC} + A \cdot \omega^s \tag{5}$$

where σ_{DC}—is the DC conductivity, $A\omega^s$- is the AC conductivity σ_{AC}, while A and s are constants that depend on the temperature and composition of the sample. The DC conductivity (σ_{DC}) was determined as $4.02E^{-5}$ $(\Omega m)^{-1}$, pre-exponential factor (A) as $7.31\ E^{-9}$, and the frequency exponent (s) as 0.92 (values lie between 0 and 1 [22]). The value of $0 < s < 1$ signifies the widely observed behavior in disordered materials (solid-state materials, ceramic samples, ionic electrolytes, ionic conducting glasses, conducting polymers, amorphous semiconductors) associated with hopping conduction known as 'the universal dynamic response' [33, 40–43]. The determined value for s of 0.92 shows the hopping behavior of charge careers of Aloe vera. The plot is characterized by a flat plateau in the low-frequency regime related to σ_{DC} and dispersion at high frequencies termed the frequency-dependent conductivity. The mechanism of conductivity in the frequency domain can be associated with the relaxation of the ionic atmosphere accompanied by mobile charge carriers [44]. The variation of conductivity is in agreement with the ε': a high dielectric constant in low-frequency region accounts for strong dielectric polarization (high ε') which is attributed to low DC conductivity and lower polarization (low ε') in a high-frequency regime causes large σ_{AC}.

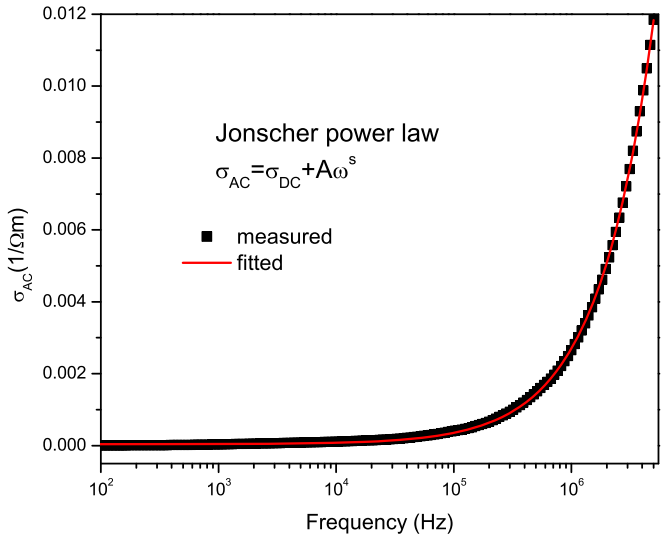

Figure 8. Frequency dependence of electrical conductivity determined using equation (4) for measured Aloe vera leaf sample.

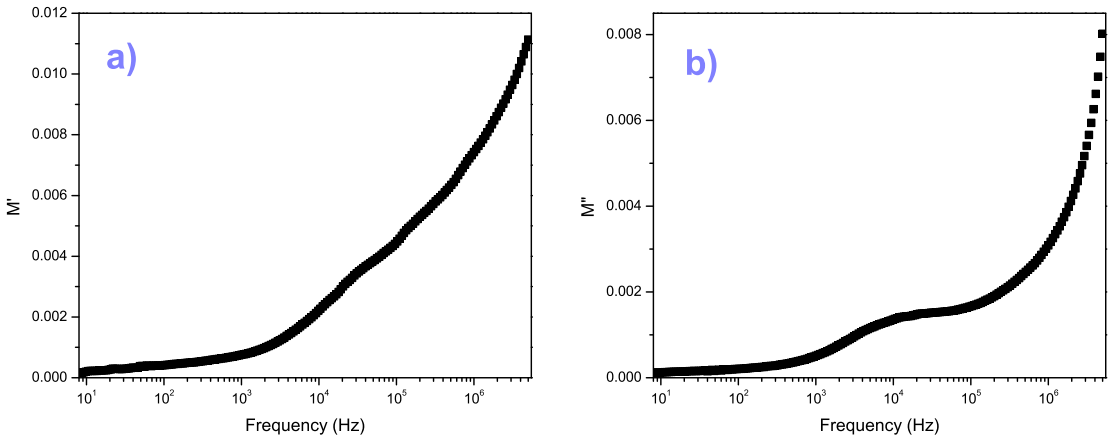

Figure 9. Frequency dependence of real (M′) and imaginary (M″) component of electric modulus M* determined using equation (6) for Aloe vera leaf sample.

3.5. Electric modulus

The complex electric modulus can be defined as the inverse of complex permittivity ε^* [45]:

$$M^* = (\varepsilon^*) - 1 = (\varepsilon' - i\varepsilon'') - 1, \text{ thus } M' = \frac{\varepsilon'}{\varepsilon'^2 + \varepsilon''^2} \text{ and } M'' = \frac{\varepsilon''}{\varepsilon'^2 + \varepsilon''^2} \quad (6)$$

where M'-real part, M''-imaginary part of M^*. Both M' and M'' reveal the electrical transport mechanism associated with carrier/ion hopping and differentiate grain boundary conduction from electrode polarization. The electrical modulus is utilized to explore the electrical phenomenon due to small capacitance of the material. Analysis of the change of electric modulus with frequency enables a better insight into the conductivity relaxation process of the analyzed material. It also evaluates the electrical relaxation in ionic solids, as the modulus change can be associated with the decay of the electric field under the influence of a constant dielectric displacement [45, 46]. The determined change of modulus with frequency is shown in figure 9.

Both real (M') and imaginary (M'') components of the electric modulus increase as the frequency increases from 8 Hz to 5 MHz. They are low in the low-frequency regime and this indicates a small contribution of electrode polarization that can be connected with the long-range mobility of charge carriers [47]. After 1 KHz, we can observe a rapid increase in M' towards saturation associated with the contribution of grains (intra-grain) at high frequencies. It agrees with the fact that the conduction process is dependent on the short-range mobility of charge carriers [48]. It plausibly relates to the lack of restoring force responsible for the mobility of charge carriers due to the induced electric field.

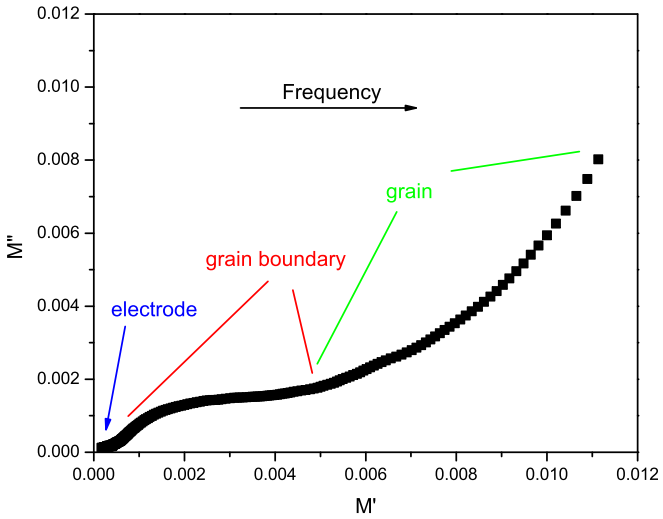

Figure 10. Complex electric modulus determined using equation (6) for Aloe vera leaf sample.

The plot of M'' demonstrates a peak lying in the middle of the frequency region centered around 10 KHz and a steep rise is observed in M'' after the trailing edge of the peak. The territory from low to a high-frequency region of the M'' peak relates to the changeover from long-range mobility to a short-range one. In the low-frequency region, charge carriers have mobility along large distances, and small-distance mobility is present in the high-frequency region. More specifically, we can see a noticeable semicircle in the lower frequency region that reflects the grain boundary influence in the form of a depressed semicircle, and higher values in the higher frequency region. The asymmetric and broad nature of the semicircle confirms non-Debye relaxation behavior. It is noteworthy that trends of M', σ and ε' agree with each other. High polarization in the low-frequency regime causes large ε', low conductivity M' and σ_{dc}, and vice-versa.

The determined loss tangent for Aloe vera leaf sample (figure 7) shows one full relaxation peak at frequencies (100 Hz–100 kHz) and the leading part of a second partial relaxation peak at high frequencies (100 kHz–5 MHz). Analysis of the Nyquist plots of electric modulus (M'-M'') enables better discrimination between electrode polarization and grain boundary conduction processes [49], as shown in figure 10.

In the M'-M'' plots, conductivity relaxation due to the semi-circle observed in the low-frequency region is responsible for the first peak of the loss tangent, thus grain boundaries contribute to this relaxation: as mentioned before, the low frequency electron 'spike' noted in the frequency range 8–100 Hz in $Z'(R)$-$Z''(X)$ plots (figure 5) is due to electrode polarization. The observed grain boundary relaxation is non-Debye type due to its asymmetric nature with the center lying below the x-axis. The leading part of the second partial peak of loss tangent displayed at high frequencies is associated with the small semicircle arc in the high-frequency regime of Nyquist plots (figure 6), where the grains are responsible for dielectric relaxation. It is also observed that Nyquist plots display relatively strong conductivity relaxation in M'-M'' plots than dielectric relaxation for Z'-Z'' plots. This relates to the complete relaxation peak of tanδ in the former and partial relaxation peak in the latter.

Aloe vera, as a succulent plant, can survive for a long duration without watering. In the electronic/electrical domain, energy can be stored either in the form of an electric field or a magnetic field. In Aloe vera, the leaf constituents (composed of parenchyma cells, vascular bundles and other internal tissue of the rind that according to analysis of measured FTIR spectra—figure 3, constitute the same functional groups) have different shapes and the parenchyma cells constitute thin cell wall/grain boundaries with possible dimensions of the order of 300–400 μm [6]. These cells execute essential activities viz-a-viz storage, secretion, photosynthesis, transport of water, etc. Grain boundary capacitance (C_{gb}) of 50.65 nF associated with polarization formed at the grain boundary was determined (table 1). The charge carriers can accumulate at the grain boundaries and form polarization, thereby creating capacitance. Thus, the thin cell/grain boundaries of parenchyma cells could help to store the energy in the form of an electric field (capacitance). These cell/grain boundaries do not let the stored energy/capacitance discharge owing to considerable $R_{gb} = 66.42$ MΩ or large time constant τ (table 1). Hence, Aloe vera as a succulent plant could possibly store energy in an electric field created by parenchyma cells for a certain time period, which could be equivalent to its water storage retention capability. This requires further research and measurements of leaf sections of different Aloe vera plants and in different conditions over longer periods of time. Life-time, stability criteria and performance capabilities need to be taken into account.

4. Conclusion

In this work, we have measured and analyzed the complex impedance of freshly cut leaf sections of the Aloe vera plant. Measured FTIR spectrum of the freeze dried leaf section enabled identification of functional groups of the cell wall structure. The complex impedance, dielectric, and electric modulus properties of Aloe vera plant leaf internal structure have been correlated with grain and grain boundary components usual for solid-state materials, showing non-Debye dielectric/conductivity relaxation behavior. The role of grain boundaries that could be associated with parenchyma cells has been described with the help of circuit modeling enabling an electrical explanation for the water retention ability of plants. This work is a contribution to the better understanding of this natural material from an electrical viewpoint and as a natural organic dielectric, to further their electronic application.

Acknowledgments

We would like to express our gratitude to Dr Aleksandra Mitrovic (IMSI) for help with optical microscopy measurements. We acknowledge the Ministry for Science, Technological Development and Innovations of the Republic of Serbia, contracts 451–03–47/2023–1/200053 (M.V.N.) and 451–03–47/2023–1//200007 (M.B.).

Data availability statement

The data is part of ongoing research and will be made available on request and made openly available when the research is complete in a data repository. The data that support the findings of this study are available upon reasonable request from the authors. Data will be available from 3 January 2024.

ORCID iDs

Maria Vesna Nikolic https://orcid.org/0000-0001-5035-0170
Charanjeet Singh https://orcid.org/0000-0001-9799-1418
Milica Bogdanovic https://orcid.org/0000-0001-8034-2606

References

[1] Zhang Y, Bao Z, Ye X, Xie Z, He K, Mergens B, Li W, Yatchiba M and Zheng Q 2018 Chemical investigation of major constituents in Aloe vera leaves and several commercial aloe juice powders *J. AOAC Int.* **101** 1741
[2] Kumar S, Yadav M, Yadav A and Yadav J P 2017 Impact of spatial and climatic conditions on phytochemical diversity and *in vitro* antioxidant activity of Indian Aloe vera (L.) Burn. F *S. Afr. J. Bot.* **111** 50–9
[3] Silva H, Sagardia S, Ortiz M, Franck N, Opazo M, Quioz M, Baginsky C and Tapia C 2014 Relationship between leaf anatomy, morphology and water use efficiency in Aloe vera (L) Burm. F. as a function of water availability *Rev. Chil. de Hist. Nat.* **87** 13
[4] Femenia A, Sanchez E S, Simal S and Rossello C 1999 Compositional features of polysaccharides from Aloe vera (*Aloe barbadensis* Miller) plant tissues *Carbohydr. Polym.* **39** 109–17
[5] Hamman J H 2008 Composition and application of Aloe vera leaf gel *Molecules* **13** 1599–616
[6] Ni Y, Turner D, Yates K M and Tizard I 2004 Isolation and characterization of structural components of Aloe vera L. leaf pulp *Int. Immunopharmacol.* **4** 1745–55
[7] Choi S and Chung M H 2003 A review on the relationship between Aloe vera components and their biological effects *Seminars in Integrative Medicine* **1** 53–62
[8] Sanchez-Machado D I, Lopez-Cervantes J, Senson R, Sanches-Silva A and Vera A 2017 Ancient knowledge with new frontiers *Trends Food Sci. Technol.* **61** 94–102
[9] Nicolau-Lapena I, Colas-Meda P, Alegre I, Aguilo-Aghayo I, Muranyi P and Vinas I 2021 Aloe vera gel: an update on its use as a functional edible coating to preserve fruit and vegetables *Prog. Org. Coat.* **151** 106007
[10] Mondal M I H, Saha J and Rahman M A 2021 Functional applications of Aloe vera on textiles: a review *J. Polym. Environ.* **29** 993–1009
[11] Chaitanya S and Singh I 2018 Ecofriendly treatment of aloe vera fibers for PLA based green composites *Int. J. Precis. Eng. Manuf.—Green Technol.* **5** 143–50
[12] Dufil G, Bernacka-Wojcik I, Armada-Moreira A and Stavrinidou E 2023 Plant bioelectronics and biohybrids: the growing contribution of organic electronic and carbon based materials *Chem. Rev.* **122** 4847–83
[13] Meder F, Mondini A, Visentin F, Zimi G, Crepaldi M and Mazzolai B 2022 Multisource energy conversion in plants with soft epicuticular coatings *Energy Environ. Sci.* **15** 2545
[14] Sharova A S, Melloni F, Lanzani G, Bettinger C J and Caironi M 2021 Edible electronics: the vision and the challenge *Adv. Mater. Technol.* **6** 2000757
[15] Singh K and Kumar N 2021 Renewable and sustainable electrical energy harvested from living plants: an experimental study *Proc. Int. Conf. on Electrical, Computer, Communications and Mechatronics Engineering (ICECCMG)* October 7–8, Mauritius (https://doi.org/10.1109/ICECCME52200.2021.9590928)
[16] Alluri N R, Raj N P M J, Khandelwal G, Vivekanathan V and Kim S J 2020 Aloe Vera: a tropical dessert plant to harness the mechanical energy by triboelectric and piezoelelctric approaches *Nano Energy* **73** 104767

[17] Mousa M A, Soliman M A, Saleh M A and Radwan A G 2021 Tactile sensing biohybrid soft E-skin based on bioimpedance using aloe vera pulp tissues *Sci. Rep.* **11** 3054
[18] Li J H, Fan L F, Zhao D J, Zhou Q, Yao J P, Wang Z Y and Huang L 2021 Plant electrical signals: a multidisciplinary challenge *J. Plant Physiol.* **261** 153418
[19] Kim J J, Allison L K and Andrew T L 2019 Vapor-printed polymer electrodes for long-term on-demand health monitoring *Sci. Adv.* **5** eaaw0463
[20] Barbosa J A *et al* 2022 Biocompatible wearable electrodes toward on-site monitoring of water loss from plants *ACS Appl. Mater. Interfaces* **14** 22989–3001
[21] Irvine J T S, Sinclair D C and West A R 1990 Electroceramics: characterization by impedance spectroscopy *Adv. Mater.* **2** 132–8
[22] Nikolic M V, Sekulic D L, Vasiljevic Z Z, Lukovic M D, Pavlovic V B and Aleksic O S 2017 Dielectric properties, complex impedance and electrical conductivity of Fe_2TiO_5 nanopowder compacts and bulk samples at elevated temperatures *J. Mater. Sci., Mater. Electron.* **28** 4796–806
[23] Kuzmin A V, Plekhanov M S and Lesnichyova A S 2020 Influence of impurities on the bulk and grain boundary conductivity of $CaZrO_3$-based proton conducting electrolyte: a distribution of relaxation time study *Electrochim. Acta* **348** 136329
[24] Springer T E, Zawodzinski T A, Wilson M S and Gottesfeld S 1996 Characterization of polymer electrolyte fuel cells using AC impedance spectroscopy *J. Electrochem. Soc.* **143** 587
[25] Joczak I, Vegvari G and Vozary E 2019 Electrical impedance measurement on plants: a review with some insights to other fields *Theor. Exp. Plant Physiol.* **31** 359–75
[26] Garlando U, Calvo S, Barezzi M, Sangimarno A, Ros P M and Demarchi D 2022 Ask the plants directly: Understanding plant needs using electrical impedance measurements *Comput. Electron. Agric.* **193** 106707
[27] Fleig J, Pham P, Szulzaft P and Maier J 1998 Inhomogeneous current distributions at grain boundaries and electrodes and their impact on impedance *Solid State Ion.* **113-115** 739–47
[28] Dojcinovic M P, Vasiljevic Z Z, Kovac J, Tadic N B and Nikolic M V 2021 Nickel manganite-sodium alginate nano-biocomposite for temperature sensing *Chemosensors* **9** 241
[29] Choi Y M, Shin D H and Kim C H 2016 An optimized methodology to observe internal microstructures of Aloe vera by cryo-scanning electron microscope *Appl. Microsc.* **46** 76–82
[30] Dehghan S, Golipour-Kanani A, Dolatabadi M K and Bahrami S H 2022 Nanofibrous composite from polycaprolactone-Polyethylene glycol-Aloe vera as a promising scaffold for bone repairing *J. Appl. Polym. Sci.* **139** e52463
[31] Torres-Giner S, Wilkanowicz S, Melendez-Rodriguez B and Lagaron J M 2017 Nanoencapsulation of Aloe vera in synthetic and naturally occurring polymers by electrohydrodynamic processing of interest in food technology and bioactive packaging *J. Agric. Food Chem.* **65** 4439–48
[32] Bajer D, Janczak K and Bajer K 2020 Novel starch/chitosan/Aloe vera composites as promising biopackaging materials *J. Polym. Environ.* **28** 1021–39
[33] Slankamenac M, Ivetic T, Nikolic M V, Ivetic N, Zivanov M and Pavlovic V B 2010 Impedance response and dielectric relaxation in liquid phase sintered Zn_2SnO_4-SnO_2 ceramics *J. Electron. Mater.* **39** 447
[34] Hona R K, Dhalimal G S and Thapa R 2022 Investigation of grain, grain boundary and interface contributions on the impedance of Ca_2FeO_5 *Appl. Sci.* **2** 2930
[35] Bondarenko A S and Ragoisha G (2016) *EIS Spectrum Analyzer* http://abc.chemistry.bsu.by
[36] Bae J M and Steele B C H 1998 Properties of $La_{0.6}Sr_{0.4}Co_{0.2}Fe_{0.8}O_{3-\delta}$ double layer cathodes on gadolinium doped cerium oxide (CGO) electrolytes *Solid State Ion.* **106** 247–53
[37] Omri K, Najeh I and El Mir L 2016 Influence of annealing temperature on the microstructure and dielectric properties of ZnO nanoparticles *Ceram. Int.* **42** 8940–8
[38] Aherrao D S, Singh C, Mathe V L, Maji P K and Srivastava A K 2023 Investigation of structural, morphological, electric modulus, AC conductivity characteristics, and validation of software-based simulated impedance/material parameters of bi-component Co-Al doped Ba-Sr ferrites, *Phys. Scr.* **98** 015813
[39] Chaudhari H N, Dhruv P N, Singh C, Meena S S, Kavita S and Jotania R B 2020 Effect of heating temperature on structural, magnetic, and dielectric properties of magnesium ferrites prepared in the presence of *Solanum Lycopersicum* fruit extract *J. Mater. Sci., Mater. Electron.* **31** 18445–63
[40] Jonscher A K 1972 Frequency dependence of conductivity in hopping systems *J. Non-Cryst. Solids* **8-10** 293–315
[41] Funke K 1993 Jump relaxation in solid electrolytes *Prog. Solid State Chem.* **22** 111–95
[42] Lee W K, Liu J F and Nowick A S 1991 Limiting behavior of ac conductivity in ionically conducting crystals *Phys. Rev. Lett.* **67** 1559–61
[43] Elliott S R 1987 A.C. conduction in amorphous chalcogenide and pnictide semiconductors *Adv. Phys.* **36** 135–217
[44] Barsoukov E and Ross Macdonald J 2005 *Impedance Spectroscopy Theory, Experiment and Applications* 2nd edn (Hoboken, New Jersey: Wiley Interscience) (https://doi.org/10.1002/0471716243)
[45] Richert R and Wagner H 1998 The dielectric modulus: relaxation versus retardation *Solid State Ion.* **105** 167–73
[46] Arun Kumar D, Selvasekarapandian S and Nithya H 2010 Dielectric, modulus and impedance analysis of LaF_3 nanoparticles *Physica* B **405** 3803–7
[47] Alptekin S, Tataroglu A and Altidunal S 2019 Dielectric, modulus and conductivity studies of Au/PVP/n-Si (MPS) structure in the wide range of frequency and voltage at room temperature *J. Mater. Sci., Mater. Electron.* **30** 6853–9
[48] Padmasree K P, Kanchan D K and Kulkarni A R 2006 Impedance and modulus studies of the solid electrolyte system $20CdI_2$–$80[xAg_2O$–$y(0.7V_2O_5$–$0.3B_2O_3)]$, where $1 \leqslant x/y \leqslant 3$ *Solid State Ion.* **177** 475–82
[49] Joshi J H, Kanchan D K, Joshi M J, Jethva H O and Parikh K D 2017 Dielectric relaxation, complex impedance and modulus spectroscopic studies of mix phase rod like cobalt sulfide nanoparticles *Mater. Res. Bull.* **93** 63–73